Nonaffine displacements in crystalline solids in the harmonic limit

Saswati Ganguly,[1] Surajit Sengupta,[1,2] Peter Sollich,[3] and Madan Rao[4,5]
[1]*Indian Association for the Cultivation of Science, 2A & 2B Raja S. C. Mullick Road, Jadavpur, Kolkata 700032, India*
[2]*TIFR Centre for Interdisciplinary Sciences, 21 Brundavan Colony, Narsingi, Hyderabad 500075, India*
[3]*King's College London, Department of Mathematics, Strand, London WC2R 2LS, United Kingdom*
[4]*Raman Research Institute, C.V. Raman Avenue, Bangalore 560080, India*
[5]*National Centre for Biological Sciences (TIFR), Bellary Road, Bangalore 560 065, India*
(Received 26 December 2012; published 2 April 2013)

A systematic coarse graining of microscopic atomic displacements generates a local elastic deformation tensor D as well as a positive definite scalar χ measuring *nonaffinity*, i.e., the extent to which the displacements are not representable as affine deformations of a reference crystal. We perform an exact calculation of the statistics of χ and D and their spatial correlations for solids at low temperatures, within a harmonic approximation and in one and two dimensions. We obtain the joint distribution $P(\chi,\mathsf{D})$ and the two-point spatial correlation functions for χ and D. We show that nonaffine and affine deformations are coupled even in a harmonic solid, with a strength that depends on the size of the coarse-graining volume Ω and dimensionality. As a corollary to our work, we identify the field h_χ conjugate to χ and show that this field may be tuned to produce a transition to a state where the ensemble average $\langle\chi\rangle$ and the correlation length of χ diverge. Our work should be useful as a template for understanding nonaffine displacements in realistic systems with or without disorder and as a means for developing computational tools for studying the effects of nonaffine displacements in melting, plastic flow, and the glass transition.

DOI: 10.1103/PhysRevE.87.042801 PACS number(s): 62.20.D−, 63.50.Lm, 63.10.+a

I. INTRODUCTION

Understanding the mechanical response of soft and disordered solids [1] such as polymer gels [2], fabric [3], foams [4], colloids [5], granular matter [6], and glasses [7,8] is challenging because one is often led to questions that lie on the boundaries of classical elasticity theory [9–11]. For example, under external stress, particles i within a solid undergo displacements $\mathbf{u}_i = \mathbf{r}_i - \mathbf{R}_i$ away from some chosen reference configuration $\mathbf{R}_i$ to their displaced positions $\mathbf{r}_i$. In a conventional homogeneous solid, such displacements are *affine*, in the sense that they can be expressed as $\mathbf{u}_i = \mathsf{D}\mathbf{R}_i$, where $\mathsf{D} = \mathsf{K}^{-1}\sigma$ is the deformation tensor related to the external stress σ via the tensor of elastic constants K. This is not true if the solid is disordered at a microscopic level.

One of the principal sources of *nonaffinity* is a space (and possibly even time) dependent elastic constant [12]. The local environment in a disordered solid varies in space, depending crucially on local connectivity or coordination such that the local displacement $\mathbf{u}_i$ may not be simply related to the applied stress σ. Such nonaffine displacements are present even at zero temperature, are material dependent, and vanish only for homogeneous crystalline media without defects.

In this paper we explore another, perhaps complementary, source of nonaffinity, namely, that which arises due to thermal fluctuations and coarse graining. Elastic properties of materials emerge upon coarse graining microscopic particle displacements [13–19] over a coarse-graining volume Ω. A systematic finite size scaling analysis of the Ω dependent elastic constants then yields the material properties in the thermodynamic limit [17,18]. Such a coarse-graining procedure has been used to obtain elastic constants of soft colloidal crystals from video microscopy [16,17,19] as well as in model solids [13,18]. For distances smaller than the size of Ω, particle displacements, in d dimensions, are necessarily *nonaffine* since the local distortion D of Ω is obtained by projecting the displacements of all N particles in Ω into the $d \times d$-dimensional space of affine distortions which, in general, is smaller than the full Nd-dimensional configuration space available. The generation of nonaffinity χ, defined as the sum of squares of all the particle displacements which do not belong to the projected space of affine distortions, is therefore a necessary consequence of the coarse-graining procedure. Here we take a detailed look at this process and present an exact calculation for the probability distributions and correlation functions for χ and D for harmonic solids in $d = 1$ and 2 in the canonical ensemble. Our work allows us to identify the field conjugate to χ, viz., h_χ, and we show that by tuning this h_χ one may enhance nonaffine fluctuations and cause a transition. At this transition all the moments of the probability distribution of χ diverge, thereby disordering the solid *isothermally*.

There are several reasons why we believe that our work may be useful. First, the harmonic crystal is often the starting point for more realistic calculations of the elastic properties of solids and constitutes an ideal system to which simulation and experimental results [20] can be compared in order to quantify purely anharmonic effects. Secondly, a coarse-grained theory for the mechanical properties of soft solids should contain both the elastic and nonelastic fields D and χ: Our work may provide a hint on how such a theory may be constructed. Thirdly, we believe that it may be possible to extend our calculations to systems with isolated defects or randomness, thus extending the analysis of Ref. [12] to nonzero temperatures. Finally, our calculations may be used to devise new simulational strategies for understanding the influence of nonaffine fluctuations on the mechanical properties of both crystals and glasses and, perhaps, shed more light on the nature of the glass transition itself.

The paper is organized as follows. In Sec. II we set up the calculation and define χ, D, and the coarse-graining process.

In Sec. III we present our calculation for the single-point probability distributions for χ and D for $d = 1$ harmonic chains and the $d = 2$ triangular harmonic lattices. Approximate experimental realizations of these systems correspond to mercury chain salts [21] and the spectrin network in red blood corpuscles [22], respectively. In Sec. IV, we evaluate the spatial correlation functions for D and χ. This is followed by a calculation of linear response and identification of the nonaffine field in Sec. V. Finally we discuss our results and conclude by giving indications of future directions in Sec. VI.

II. COARSE GRAINING AND THE NONAFFINE PARAMETER

Consider a neighborhood Ω in a d-dimensional lattice consisting of N particles i arranged around the central particle 0 within a cut-off distance R_Ω. Mostly we set R_Ω equal to the nearest neighbor distance so that Ω contains all nearest neighbours of particle 0, but in Sec. VI we also consider larger R_Ω. The zero temperature lattice positions that we choose as our reference are $\mathbf{R}_i$ and $\mathbf{R}_0$ and the fluctuating atom positions will be denoted $\mathbf{r}_i$ and $\mathbf{r}_0$ [23]. Define the particle displacements $\mathbf{u}_i = \mathbf{r}_i - \mathbf{R}_i$ and $\boldsymbol{\Delta}_i = \mathbf{u}_i - \mathbf{u}_0 = \mathbf{r}_i - \mathbf{r}_0 - (\mathbf{R}_i - \mathbf{R}_0)$ as the displacement of particle i relative to particle 0. We will often use the Fourier transform of the particle displacement, $\mathbf{u}_\mathbf{q}$, which is defined such that the real-space displacements are $\boldsymbol{\Delta}_i = \mathbf{u}_i - \mathbf{u}_0 = l\, v_{\mathrm{BZ}}^{-1} \int d\mathbf{q}\, \mathbf{u}_\mathbf{q}(e^{i\mathbf{q}\cdot\mathbf{R}_i} - e^{i\mathbf{q}\cdot\mathbf{R}_0})$. Here l is the lattice parameter and v_{BZ} is the volume of the Brillouin zone over which the $\mathbf{q}$ integral is performed.

If the local particle displacements are fully affine, then one has $\mathbf{u}_i = \mathsf{D}\mathbf{R}_i$, and hence $\boldsymbol{\Delta}_i = \mathsf{D}(\mathbf{R}_i - \mathbf{R}_0)$. Generically the displacements will contain a nonaffine component and the coarse-grained local deformation tensor D can then be defined [8,24] as the one that minimizes $\sum_i [\boldsymbol{\Delta}_i - \mathsf{D}(\mathbf{R}_i - \mathbf{R}_0)]^2$. The minimal value of this quantity is the nonaffinity parameter χ.

To simplify the notation we arrange the Nd relative displacement components $\Delta_{i\alpha}$, where the index $\alpha = 1, \ldots, d$ labels the spatial components, into an Nd-dimensional vector $\boldsymbol{\Delta}$. We similarly define a vector $\mathbf{e}$ whose components are the d^2 elements of the local deformation tensor $\mathsf{D}_{\alpha\gamma}$ arranged as a linear array [viz., $\mathbf{e} = (D_{11}, D_{12}, \ldots, D_{1d}, D_{21}, \ldots, D_{Nd})$], and a matrix R of size $Nd \times d^2$ with elements $\mathsf{R}_{i\alpha,\gamma\gamma'} = \delta_{\alpha\gamma}(R_{i\gamma'} - R_{0\gamma'})$ where the $R_{i\gamma'}$ and $R_{0,\gamma'}$ are the components of the lattice positions $\mathbf{R}_i$ and $\mathbf{R}_i$, respectively. Below we use the notations $\mathbf{e}$ and D for the deformation tensor interchangeably, as convenient in the context.

As explained above, we will define the nonaffinity parameter χ as the residual sum of squares of all the displacements of the particles in Ω after fitting the best affine deformation, measured with respect to the reference configuration [8]. The local deformation $\mathbf{e}$ is thus obtained by minimizing the positive definite quantity $(\Delta - \mathsf{R}\mathbf{e})^2$ with respect to $\mathbf{e}$:

$$\begin{aligned}\chi &= \min_\mathbf{e} (\boldsymbol{\Delta} - \mathsf{R}\mathbf{e})^2 \\ &= \min_\mathbf{e}(\boldsymbol{\Delta}^t\boldsymbol{\Delta} - \boldsymbol{\Delta}^t\mathsf{R}\mathbf{e} - \mathbf{e}^t\mathsf{R}^t\boldsymbol{\Delta} + \mathbf{e}^t\mathsf{R}^t\mathsf{R}\mathbf{e}). \end{aligned} \tag{1}$$

Here the superscript t denotes the transpose operation. The coarse-grained local deformation, i.e., the value of $\mathbf{e}$ where the minimum is obtained, can then be written as

$$\mathbf{e} = \mathsf{Q}\boldsymbol{\Delta}, \tag{2}$$

where

$$\mathsf{Q} = (\mathsf{R}^t\mathsf{R})^{-1}\mathsf{R}^t. \tag{3}$$

The resulting nonaffinity χ from (1) is

$$\chi = [\boldsymbol{\Delta} - \mathsf{R}(\mathsf{R}^t\mathsf{R})^{-1}\mathsf{R}^t\boldsymbol{\Delta}]^2 = \boldsymbol{\Delta}^t\mathsf{P}\boldsymbol{\Delta}, \tag{4}$$

where

$$\mathsf{P} = \mathsf{I} - \mathsf{R}\mathsf{Q} = \mathsf{I} - \mathsf{R}(\mathsf{R}^t\mathsf{R})^{-1}\mathsf{R}^t \tag{5}$$

projects onto the space of $\boldsymbol{\Delta}$ that cannot be expressed as an affine deformation. Note that in arriving at (4) we have used the fact that P is symmetric, i.e., $\mathsf{P}^t = \mathsf{P}$ and

$$\begin{aligned}\mathsf{P}^2 &= [\mathsf{I} - \mathsf{R}(\mathsf{R}^t\mathsf{R})^{-1}\mathsf{R}^t]^2 \\ &= \mathsf{I}^2 - 2\,\mathsf{R}(\mathsf{R}^t\mathsf{R})^{-1}\mathsf{R}^t \\ &\quad + \mathsf{R}(\mathsf{R}^t\mathsf{R})^{-1}[(\mathsf{R}^t\mathsf{R})(\mathsf{R}^t\mathsf{R})^{-1}]\mathsf{R}^t \\ &= \mathsf{P}. \end{aligned} \tag{6}$$

As usual this means that all eigenvalues of P are either zero or one.

Having found explicit expressions for $\mathbf{e}$ and χ we now proceed to obtain their statistics at low temperature, where a harmonic approximation will be valid. Specifically we consider the canonical distribution of displacements $\mathbf{u}_i$ and momenta $\mathbf{p}_i$ at inverse temperature $\beta = 1/k_BT$:

$$P(\mathbf{p}_i, \mathbf{u}_i) = \frac{1}{Z}\exp[-\beta H(\mathbf{p}_i, \mathbf{u}_i)] \tag{7}$$

with the harmonic Hamiltonian

$$H = \sum_i \frac{\mathbf{p}_i^2}{2m_i} + \frac{K}{2}\sum_{(ij)}(\mathbf{u}_i - \mathbf{u}_j)^2, \tag{8}$$

where m_i is the mass of particle i. The sum in the second term in (8) runs over all bonds in a harmonic network with spring constants K. This is the Hamiltonian for the examples we consider in this paper. However, the general expressions that we derive apply directly also to generic quadratic Hamiltonians of the form

$$H = \sum_i \frac{\mathbf{p}_i^2}{2m_i} + \frac{1}{2\beta l^2}\sum_{i\alpha j\gamma} u_{i\alpha}\mathcal{D}_{i\alpha,j\gamma}u_{j\gamma}. \tag{9}$$

Here $\mathcal{D}_{i\alpha,j\gamma}$ is the dynamical matrix; we have made this dimensionless by extracting a factor of $1/(\beta l^2)$.

Integrating out the momenta from the canonical distribution shows that the particle displacements have a Gaussian distribution. Their covariances can be expressed compactly in terms of the Fourier transform of the dynamical matrix [25,26]

$$\tilde{\mathcal{D}}_{\alpha\gamma}(\mathbf{q}) = \sum_i \mathcal{D}_{i\alpha,j\gamma}e^{-i\mathbf{q}\cdot(\mathbf{R}_i - \mathbf{R}_j)}, \tag{10}$$

where because of translational invariance the choice of reference particle j is arbitrary. This matrix determines the variances of the Fourier components according to

$$\left\langle \mathbf{u}_\mathbf{q}\mathbf{u}_{-\mathbf{q}'}^t \right\rangle = \tilde{\mathcal{D}}^{-1}(\mathbf{q})\, v_{\mathrm{BZ}}\delta(\mathbf{q} - \mathbf{q}'), \tag{11}$$

where the angle brackets indicate a thermal average. The covariances of the displacements are, accordingly,

$$\langle \mathbf{u}_i \mathbf{u}_j^t \rangle = l^2 \int \frac{d\mathbf{q}}{v_{\mathrm{BZ}}} \tilde{\mathcal{D}}^{-1}(\mathbf{q})\, e^{i\mathbf{q}\cdot(\mathbf{R}_i - \mathbf{R}_j)}. \tag{12}$$

For the particle displacements in our coarse-graining volume Ω of interest, $\mathbf{\Delta}_i = \mathbf{u}_i - \mathbf{u}_0$, we thus find also a Gaussian distribution with covariance matrix $\langle \Delta_{i\alpha} \Delta_{j\gamma} \rangle$ given by

$$C_{i\alpha,j\gamma} = l^2 \int \frac{d\mathbf{q}}{v_{\mathrm{BZ}}} \tilde{\mathcal{D}}^{-1}_{\alpha\gamma}(\mathbf{q})(e^{i\mathbf{q}\cdot\mathbf{R}_j} - e^{i\mathbf{q}\cdot\mathbf{R}_0}) \times (e^{-i\mathbf{q}\cdot\mathbf{R}_i} - e^{-i\mathbf{q}\cdot\mathbf{R}_0}). \tag{13}$$

Note that the matrix C defined in this way has the symmetry of the lattice. The thermal average of any observable $A(\Delta)$ is then given by

$$\langle A \rangle = \frac{1}{Z_\Omega} \int \prod_{i\alpha} d\Delta_{i\alpha}\, A(\mathbf{\Delta}) \exp\left(-\frac{1}{2}\mathbf{\Delta}^t \mathsf{C}^{-1} \mathbf{\Delta}\right) \tag{14}$$

with normalization constant $Z_\Omega = (2\pi)^{Nd/2}\sqrt{\det \mathsf{C}}$. In the next section we use (14) to obtain the probability distribution functions for χ and $\mathbf{e}$.

III. SINGLE-POINT PROBABILITY DISTRIBUTIONS

In this section we derive the single-point (local) joint probability distribution $P(\chi,\mathbf{e})$ for nonaffinity χ and strains $\mathbf{e}$. As before we consider lattices at nonzero but low temperatures where a harmonic approximation to particle interactions remains valid. To obtain $P(\chi,\mathbf{e})$, we begin with

$$\Phi(k,\boldsymbol{\kappa}) = \int d\chi\, d\mathbf{e}\, P(\chi,\mathbf{e}) \exp(ik\chi + i\boldsymbol{\kappa}^t \mathbf{e}) = \langle e^{ik\chi + i\boldsymbol{\kappa}^t \mathbf{e}} \rangle, \tag{15}$$

which is the characteristic function for the joint probability distribution $P(\chi,\mathbf{e})$ as measured within Ω. Substituting the general expressions from Sec. II, $\chi = \mathbf{\Delta}^t \mathsf{P} \mathbf{\Delta}$ and $\mathbf{e} = \mathsf{Q}\mathbf{\Delta}$, into (15) we obtain

$$\Phi(k,\boldsymbol{\kappa}) = \frac{1}{Z_\Omega} \int \prod_{i\alpha} d\Delta_{i\alpha} \times \exp\left[-\frac{1}{2}\mathbf{\Delta}^t \mathsf{C}^{-1} \mathbf{\Delta} + ik\mathbf{\Delta}^t \mathsf{P} \mathbf{\Delta} + i\boldsymbol{\kappa}^t \mathsf{Q} \mathbf{\Delta}\right]. \tag{16}$$

Completing the squares in the argument of the exponential in (16) and carrying out the resulting Gaussian integrals yields

$$\Phi(k,\boldsymbol{\kappa}) = \exp\left(-\frac{1}{2}\boldsymbol{\kappa}^t \mathsf{QC}(\mathsf{I} - 2ik\mathsf{PC})^{-1}\mathsf{Q}^t \boldsymbol{\kappa}\right) \times [\det(\mathsf{I} - 2ik\mathsf{PCP})]^{-1/2}. \tag{17}$$

Setting $\boldsymbol{\kappa} = 0$ and $k = 0$ gives the characteristic functions of χ and $\mathbf{e}$, respectively, as

$$\Phi_\chi(k) = [\det(\mathsf{I} - 2ik\mathsf{PCP})]^{-1/2}, \tag{18}$$

$$\Phi_{\mathbf{e}}(\boldsymbol{\kappa}) = \exp\left(-\tfrac{1}{2}\boldsymbol{\kappa}^t \mathsf{QCQ}^t \boldsymbol{\kappa}\right). \tag{19}$$

Extracting these factors from the joint characteristic function shows that it can be written as

$$\Phi(k,\boldsymbol{\kappa}) = \Phi_\chi(k)\Phi_{\mathbf{e}}(\boldsymbol{\kappa}) \times \exp[-ik\boldsymbol{\kappa}^t \mathsf{QC}(\mathsf{I} - 2ik\mathsf{PC})^{-1}\mathsf{PCQ}^t \boldsymbol{\kappa}]. \tag{20}$$

The term in the second line expresses the fact that χ and $\mathbf{e}$ are generally coupled to each other, rather than varying independently. A special case where this does not happen occurs when P and C commute. Then one can write $\mathsf{PCQ}^t = \mathsf{CPQ}^t$. But this vanishes because from the definitions of P and Q one has $\mathsf{PQ}^t = 0$. The coupling term in (20) then becomes unity and χ and $\mathbf{e}$ are uncorrelated. This is the situation we will encounter in the one-dimensional example below, when coarse graining on the smallest length scale where Ω only contains the nearest neighbors of particle 0.

In the case where P and C have a nonzero commutator $[\mathsf{P},\mathsf{C}] = \mathsf{PC} - \mathsf{CP}$, one can put the expansion for small k of the coupling factor in (20) into a form that emphasizes the role of this commutator. Specifically, by writing $\mathsf{PC} = \mathsf{CP} - [\mathsf{P},\mathsf{C}]$ and exploiting the property $\mathsf{PQ}^t = 0$ one finds

$$\Phi(k,\boldsymbol{\kappa}) = \Phi_\chi(k)\Phi_{\mathbf{e}}(\boldsymbol{\kappa}) \exp(-i\boldsymbol{\kappa}^t \mathsf{QC}[[\mathsf{P},\mathsf{C}]\, k + 2i([\mathsf{CP},[\mathsf{P},\mathsf{C}]] + [\mathsf{P},\mathsf{C}]^2)\, k^2 + \cdots]\mathsf{Q}^t \boldsymbol{\kappa}). \tag{21}$$

From the general form (20) of the characteristic function, or its expanded version (21), we can then obtain the desired joint probability distribution $P(\chi,\mathbf{e})$ by inverse Fourier transform, either analytically or numerically.

Before proceeding to apply the above general results to two simple example systems, we comment briefly on the marginal distributions of χ and $\mathbf{e}$ whose characteristic functions are given in (18) and (19) above. From the second of these equations, the distribution $P(\mathbf{e})$ of the local strain is a zero mean Gaussian distribution with covariance matrix QCQ^t. For the local nonaffinity χ, if we call σ_j the eigenvalues of the matrix PCP, then the characteristic function (18) has the explicit form

$$\Phi_\chi(k) = \frac{1}{\prod_j \sqrt{1 - 2ik\sigma_j}}. \tag{22}$$

This shows that χ has a generalized chi-square distribution $P(\chi)$: It is a sum of squares of Gaussian random variables, each with zero mean and variance σ_j. Only the nonzero σ_j contribute here, and there are $Nd - d^2$ of these. This follows from the fact that P eliminates from the space of all relative displacements in Ω the d^2-dimensional subspace of affine displacements.

A. The one-dimensional harmonic chain

Consider a one-dimensional chain of particles of equal mass connected by harmonic springs with spring constant K and equilibrium length l as shown in Fig. 1. We choose as the coarse-graining neighborhood Ω a central particle 0 at $\mathbf{R}_0 \equiv x_0 = 0$ and its two nearest neighbors at $x_{\pm 1} = \pm l$. Fluctuating particle positions $\mathbf{R}_i \equiv x_i$ produce displacements $u_i = x_i - il$ and the vector of relative displacements is $\mathbf{\Delta}^t = (u_1 - u_0\,, u_{-1} - u_0)$. The matrices defined in Sec. II can be easily evaluated for this system and are given by

$$\mathsf{R} = \begin{pmatrix} l \\ -l \end{pmatrix}, \quad \mathsf{Q} = (\mathsf{R}^t\mathsf{R})^{-1}\mathsf{R}^t = \begin{pmatrix} \frac{1}{2l} & -\frac{1}{2l} \end{pmatrix},$$

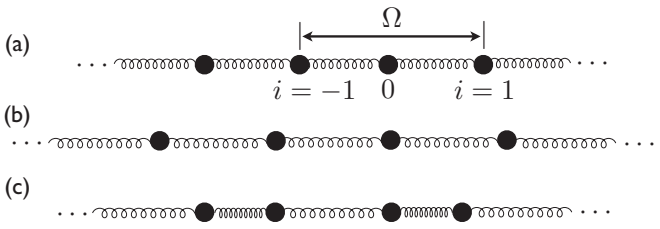

FIG. 1. (a) A portion of a one-dimensional harmonic chain showing the neighborhood Ω consisting of particle 0 and its two nearest neighbors $i = \pm 1$. The affine (b) and the nonaffine (c) modes are also shown.

and

$$\mathsf{P} = \mathsf{I} - \mathsf{R}(\mathsf{R}^t\mathsf{R})^{-1}\mathsf{R}^t = \begin{pmatrix} \frac{1}{2} & \frac{1}{2} \\ \frac{1}{2} & \frac{1}{2} \end{pmatrix}.$$

The two eigenvectors of P corresponding to the eigenvalues zero and one are $(l, -l)$ and (l,l), respectively. The mode with the nonzero eigenvalue corresponds to the nonaffine deformation $\chi = (u_1 + u_{-1} - 2u_0)^2/2$, while the one corresponding to the null space of P gives the only affine mode $\mathbf{e} = \epsilon = (u_1 - u_{-1})/2l$ of the lattice. The affine and the nonaffine modes with respect to Ω are shown in Figs. 1(b) and 1(c), respectively. The dynamical "matrix" in Fourier space is $\tilde{\mathcal{D}}(q) = 2\beta K l^2 [1 - \cos(ql)]$; in the following we use energy units such that $Kl^2 = 1$. The displacement covariance matrix (13) then becomes

$$C_{ij} = \frac{l^2}{2\beta}\frac{l}{2\pi}\int_0^{2\pi/l} dq \frac{(e^{iq\,x_i} - e^{iq\,x_0})(e^{-iqx_j} - e^{-iqx_0})}{1 - \cos(ql)}, \tag{23}$$

which is simply $l^2\beta^{-1}$ times the identity matrix and so

$$\mathsf{PCP}^t = l^2\beta^{-1}\begin{pmatrix} \frac{1}{2} & \frac{1}{2} \\ \frac{1}{2} & \frac{1}{2} \end{pmatrix}$$

with eigenvalues $\sigma = l^2\beta^{-1}$ and 0, while $\mathsf{QCQ}^t = \langle\epsilon^2\rangle = \beta^{-1}/2$.

The fact that $C_{ij} = l^2\beta^{-1}\delta_{ij}$ as found above means that the relative particle displacements are uncorrelated. This is easy to see intuitively as the potential energy of the system is $(K/2)\sum_{n=-\infty}^{\infty}(x_{n+1} - x_n - l)^2$. Relative displacements $x_{n+1} - x_n - l$ of nearest neighbors therefore have independent fluctuations, and the relative displacements $u_1 - u_0 = x_1 - x_0 - l$ and $u_{-1} - u_0 = -(x_0 - x_{-1} - l)$ in our coarse-graining neighborhood Ω are exactly of this form. If we were to enlarge Ω, say to include next-nearest neighbors, then this would no longer hold as, e.g., $u_2 - u_0 = x_2 - 2l - x_0 = (x_2 - x_1 - l) + (x_1 - x_0 - l)$ is correlated with $u_1 - u_0$.

Carrying out the matrix manipulations in (17) after specializing to the $d = 1$ case, we find that the k dependence of the first factor cancels out since $[\mathsf{P},\mathsf{C}] = 0$, in line with the general discussion after (21). This yields the characteristic function for the joint probability distribution as the product of the individual characteristic functions:

$$\begin{aligned}\Phi(k,\kappa) &= \left[\frac{1}{\sqrt{1 - 2ik\sigma}}\right]\left[\exp\left(-\frac{1}{2}\langle\epsilon^2\rangle\kappa^2\right)\right] \\ &= \Phi_\chi(k)\Phi_\epsilon(\kappa).\end{aligned} \tag{24}$$

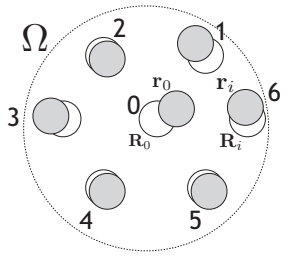

FIG. 2. A typical neighborhood Ω around a central particle 0 in a triangular lattice, containing the six nearest neighbor particles $i = 1, \ldots, 6$. The reference positions $\mathbf{R}_0$ and $\mathbf{R}_i$ are shown by open circles, while the instantaneous positions $\mathbf{r}_0$ and $\mathbf{r}_i$ are indicated by filled gray circles.

The joint probability distribution is then obtained by inverse Fourier transforming the characteristic function:

$$\begin{aligned}P(\chi,\epsilon) &= \left[\frac{1}{\sqrt{2\pi\,\sigma}}\chi^{-1/2}\exp\left(-\frac{\chi}{2\,\sigma}\right)\right] \\ &\quad\times\left[\frac{1}{\sqrt{2\pi\langle\epsilon^2\rangle}}\exp\left(-\frac{\epsilon^2}{2\langle\epsilon^2\rangle}\right)\right] \\ &= P(\chi)P(\epsilon).\end{aligned} \tag{25}$$

This has a simple form, namely, a product of the chi-square distribution of a single Gaussian random variable and a Gaussian. We can obtain immediately, for example, the nth moments of χ, $\langle\chi^n\rangle = (2\sigma)^n\Gamma(n + \frac{1}{2})/\Gamma(\frac{1}{2})$, which are all finite. In Sec. V we show that one can define an external field h_χ that couples to χ and, for a specific value, can cause all the moments to diverge so that $P(\chi)$ crosses over to a distribution with a power-law tail.

B. The two-dimensional harmonic triangular net

The joint probability distribution of local coarse-grained strain $\mathbf{e}$ and nonaffinity χ for a two-dimensional triangular lattice can be obtained in a similar manner. We choose again a nearest neighbor (hexagonal) coarse-graining neighborhood Ω as shown in Fig. 2. To simplify the notation we also assume, without loss of generality, $\mathbf{R}_0 = \mathbf{0}$ in what follows, and take the lattice constant as our length unit so that $l = 1$. Following the lines of the one-dimensional calculation, we begin by obtaining the matrices R and P.

1. R and P

The matrix R is a 12×4 matrix encoding the position vectors of the six neighbors of the particle at the origin (see Fig. 2). Explicitly one has

$$\mathsf{R} = \begin{pmatrix} R_{11} & R_{12} & 0 & 0 \\ 0 & 0 & R_{11} & R_{12} \\ \vdots & \vdots & \vdots & \vdots \\ R_{61} & R_{62} & 0 & 0 \\ 0 & 0 & R_{61} & R_{62} \end{pmatrix}. \tag{26}$$

Here the index $\alpha = 1,2$ indicates the x and y components of the lattice positions $\mathbf{R}_i$, respectively.

To find the projection matrix $\mathsf{P} = \mathsf{I} - \mathsf{R}(\mathsf{R}^t\mathsf{R})^{-1}\mathsf{R}^t$, we substitute the above form of R into the matrix $\mathsf{R}(\mathsf{R}^t\mathsf{R})^{-1}\mathsf{R}^t$. One finds that this consists of 6×6 blocks, each of which is a 2×2 diagonal matrix of the form

$$\frac{1}{3}(R_{i1}R_{j1} + R_{i2}R_{j2})\begin{pmatrix}1 & 0\\ 0 & 1\end{pmatrix} = \frac{\mathbf{R}_i \cdot \mathbf{R}_j}{3}\begin{pmatrix}1 & 0\\ 0 & 1\end{pmatrix}.$$

The resulting P has four zero eigenvalues corresponding to the affine transformations. The eight unit eigenvalues correspond to nonaffine distortions within Ω. To identify a convenient basis for the nonaffine (eight-dimensional) eigenspace, we choose below the eigenvectors of PCP with nonzero eigenvalues. Similarly, a physically meaningful basis for the affine (four-dimensional) eigenspace is formed by the nonzero eigenvectors of $(\mathsf{I} - \mathsf{P})\mathsf{C}(\mathsf{I} - \mathsf{P})$.

2. C *and* PCP

In order to obtain the statistics of $\chi = \mathbf{\Delta}^t\mathsf{P}\mathbf{\Delta}$ and $\mathbf{e} = \mathsf{Q}\mathbf{\Delta}$ we need to calculate, as before, the eigenvectors and eigenvalues of the matrices PCP and QCQ^t. As discussed above, these are the matrices determining the characteristic functions (18) and (19) and hence the marginal distributions. We thus require the displacement correlation matrix C, which in turn is calculated from the Fourier-transformed dynamical matrix $\tilde{\mathcal{D}}(\mathbf{q})$. For the Hamiltonian (8) of a regular harmonic triangular net of particles with spring constant K and lattice constant l this is

$$\tilde{\mathcal{D}}(\mathbf{q}) = \beta\begin{pmatrix}3 - 2\cos(q_x) - \cos\left(\frac{1}{2}q_x\right)\cos\left(\frac{\sqrt{3}}{2}q_y\right) & \sqrt{3}\sin\left(\frac{1}{2}q_x\right)\sin\left(\frac{\sqrt{3}}{2}q_y\right)\\ \sqrt{3}\sin\left(\frac{1}{2}q_x\right)\sin\left(\frac{\sqrt{3}}{2}q_y\right) & 3\left[1 - \cos\left(\frac{1}{2}q_x\right)\cos\left(\frac{\sqrt{3}}{2}q_y\right)\right]\end{pmatrix}. \tag{27}$$

Here we have again chosen energy units such that $Kl^2 = 1$. We also use the more intuitive notation $q_x \equiv q_1$ and $q_y \equiv q_2$ for the wave vector components.

The elements of the real symmetric matrix C are obtained by evaluating the integral (13) over the Brillouin zone of the triangular lattice. It can be shown, by utilizing lattice symmetries, that the integral can be transformed to one over a rectangular region:

$$C_{i\alpha,j\gamma} = \frac{1}{2v_{\mathrm{BZ}}}\int_0^{4\pi} dq_x \int_0^{4\pi/\sqrt{3}} dq_y\, \tilde{\mathcal{D}}^{-1}_{\alpha\gamma}(q_x,q_y) \times (e^{i\mathbf{q}\cdot\mathbf{R}_i} - e^{i\mathbf{q}\cdot\mathbf{R}_0})(e^{-i\mathbf{q}\cdot\mathbf{R}_j} - e^{-i\mathbf{q}\cdot\mathbf{R}_0}) \tag{28}$$

We compute both the real and the imaginary parts of this two-dimensional integral numerically, using 256-point Gauss-Legendre quadrature. The imaginary parts of the elements of C vanish and provide an estimate for the accuracy of our numerics. The normalizing volume of the unit cell in the reciprocal lattice is $v_{\mathrm{BZ}} = \frac{8\pi^2}{\sqrt{3}}$. C is a 6×6 block matrix, with each block of size 2×2 as before. Of course not all of these 36 blocks need to be calculated independently, because of the overall symmetry $\mathsf{C} = \mathsf{C}^t$. Using also the additional symmetry relations (see Fig. 2)

$$\begin{aligned} &C_{1\alpha1\gamma} = C_{4\alpha4\gamma}, \quad C_{2\alpha2\gamma} = C_{5\alpha5\gamma}, \quad C_{3\alpha3\gamma} = C_{6\alpha6\gamma},\\ &C_{1\alpha2\gamma} = C_{4\alpha5\gamma}, \quad C_{2\alpha3\gamma} = C_{5\alpha6\gamma}, \quad C_{3\alpha4\gamma} = C_{6\alpha1\gamma},\\ &C_{1\alpha3\gamma} = C_{4\alpha6\gamma}, \quad C_{2\alpha4\gamma} = C_{5\alpha1\gamma}, \quad C_{3\alpha5\gamma} = C_{6\alpha2\gamma}, \end{aligned} \tag{29}$$

one finds that only 12 blocks of C are distinct.

With P and C in hand one can construct and diagonalize PCP. This has 12 eigenvalues σ_j $(j = 1, \ldots, 12)$, four of which are zero. The eight nonzero eigenvalues, which correspond to the nonaffine distortions within Ω shown in Fig. 3, are

$$\begin{aligned} &\beta\sigma_1 = 2.454 = \beta\sigma_2, \quad \beta\sigma_3 = 0.482,\\ &\beta\sigma_4 = 0.312 = \beta\sigma_5, \quad \beta\sigma_6 = 0.283 = \beta\sigma_7 = \beta\sigma_8. \end{aligned} \tag{30}$$

The structure of the four-dimensional null space of PCP can be understood by looking at the nonzero eigenvectors of the matrix obtained by the complementary projection, viz., $(\mathsf{I} - \mathsf{P})\mathsf{C}(\mathsf{I} - \mathsf{P})$. These eigenvectors correspond to the affine eigendisplacements shown in Fig. 4.

The independently fluctuating "directions" of the local deformation tensor $\mathbf{e}$ can be worked out from the covariance matrix QCQ^t of the Gaussian distribution of $\mathbf{e}$ [see (19)]. The projections of $\mathbf{e}$ onto these directions then have familiar forms and map (see below) to the affine eigendistortions in Fig. 4. Explicitly we find for these projections: (a) volume change (dilation), $e_v = e_1 + e_4 = D_{11} + D_{22}$, (b) uniaxial strain, $e_u = e_1 - e_4 = D_{11} - D_{22}$, (c) shear strain, $e_s = e_2 + e_3 = D_{12} + D_{21}$, and (d) local rotation, $\omega = e_2 - e_3 = D_{12} - D_{21}$. The associated eigenvalues give the relevant compliances for our coarse-graining volume Ω:

$$\beta\langle e_v^2\rangle = 0.261, \quad \beta\langle e_u^2\rangle = 0.481 = \beta\langle e_s^2\rangle, \quad \beta\langle\omega^2\rangle = 0.699. \tag{31}$$

The statistics of the local deformation tensor $P(\mathbf{e})$ therefore consists of independent Gaussian fluctuations of these four deformation modes, as illustrated in Fig. 5(b).

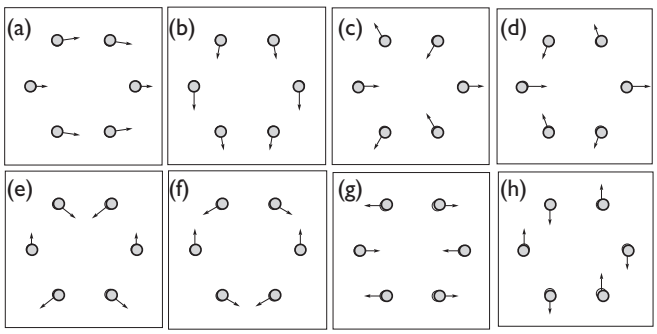

FIG. 3. Configurations showing the nonzero eigenvectors of PCP, which represent nonaffine displacements, corresponding to eigenvalues in descending order: (a) and (b) $\sigma_1 = \sigma_2$; (c) σ_3; (d) and (e) $\sigma_4 = \sigma_5$; (f)–(h) $\sigma_6 = \sigma_7 = \sigma_8$.

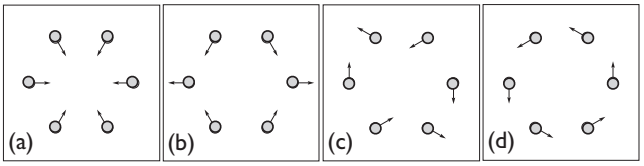

FIG. 4. Particle displacements for the nonzero eigenvectors of the matrix $(\mathsf{I}-\mathsf{P})\mathsf{C}(\mathsf{I}-\mathsf{P})$, showing affine eigendisplacements (a) dilation, (b) uniaxial strain, (c) shear, and (d) rotation. The reference lattice positions are shown by filled circles. The central atom has been deleted for clarity.

To finish our discussion of the affine displacements we comment briefly on the relation between the eigenvectors of $(\mathsf{I}-\mathsf{P})\mathsf{C}(\mathsf{I}-\mathsf{P})$, which give the independently fluctuating displacement patterns in the affine subspace ("affine eigendisplacements"), and the eigenvectors of QCQ^t, which are the independently fluctuating components of the local deformation tensor ("eigendistortions"). The two matrices are related via

$$(\mathsf{I}-\mathsf{P})\mathsf{C}(\mathsf{I}-\mathsf{P}) = \mathsf{R}(\mathsf{QCQ}^t)\mathsf{R}^t. \tag{32}$$

In the discussion above we treated their eigenvectors on the same footing, and indeed each eigendistortion $\hat{\mathbf{e}}$ as an eigenvector of QCQ^t is related to an affine eigendisplacement given by $\hat{\mathbf{\Delta}} = \mathsf{R}\hat{\mathbf{e}}$. This works, i.e., $\mathsf{R}\hat{\mathbf{e}}$ is indeed an eigenvector of (32), because $\mathsf{R}^t\mathsf{R}$ is a multiple of the identity matrix in the two-dimensional triangular net. This simplification will hold in all lattices with sufficiently high symmetry. Indeed, one can check that $\mathsf{R}^t\mathsf{R}$ has a $d\times d$ block structure where the off-diagonal blocks are zero and the diagonal blocks are all equal to $\sum_i \mathbf{R}_i\mathbf{R}_i^t$. This diagonal block is a matrix that commutes with the entire symmetry group of the lattice so by Schur's lemma [27] will be proportional to the identity matrix, unless the symmetry group of the lattice is too small.

Next we look at the statistics of the nonaffinity parameter χ. The characteristic function (18) can be written out explicitly as in (22) where the σ_j's are the eigenvalues of PCP. As we saw above, this matrix has eight nonzero eigenvalues

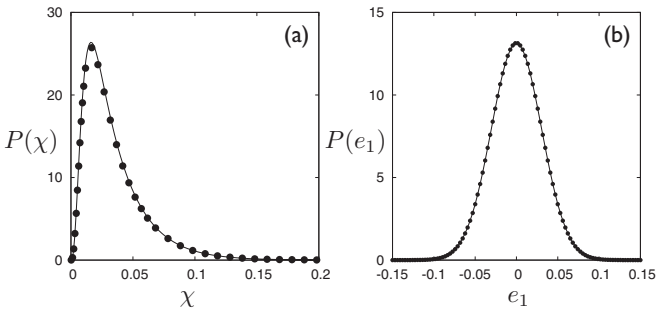

FIG. 5. (a) $P(\chi)$ from the exact calculation (line) compared with that obtained from molecular dynamics simulations (points) of a 400×400 site harmonic lattice with unit particle masses at reduced inverse temperature $\beta = 200$. The system was allowed to equilibrate for 2×10^5 MD steps with a time step of 10^{-3}, after which configurations were collected for 7×10^5 MD steps. (b) Plot of $P(e_1)$ for the same system as in (a).

$\sigma_1,\ldots,\sigma_8$ and four zero eigenvalues $\sigma_9 = \cdots = \sigma_{12} = 0$ that do not contribute to (22) as they correspond to purely affine distortions within Ω. The eigenvectors associated with the eight nonaffine displacements are shown in Fig. 3. Thus, as discussed above in general terms, $P(\chi)$ is the distribution of the sum of the squares of $Nd - d^2 = 8$ uncorrelated Gaussian random variables, with the variances of these Gaussians given by the eigenvalues $\sigma_1,\ldots,\sigma_8$. A numerical Fourier transform of (22) then gives $P(\chi)$. The result is shown in Fig. 5(a), where we also compare with data from molecular dynamics (MD) simulations; the agreement is evidently very good.

The first and the second moments of χ may be obtained from successive derivatives of $\Phi_\chi(k)$ with respect to its argument so that $\langle\chi\rangle = i^{-1}[d\Phi_\chi(k)/dk]_{k=0} = \sum_{j=1}^8 \sigma_j = 6.865\beta^{-1}$ and

$$\begin{aligned}\langle\chi^2\rangle - \langle\chi\rangle^2 &= -\left(\frac{d^2}{dk^2}\Phi_\chi(k)\right)_{k=0} - \langle\chi\rangle^2\\ &= 2\sum_{j=1}^{8}\sigma_j^2\\ &= 25.426\,\beta^{-2}.\end{aligned} \tag{33}$$

The values for the corresponding quantities obtained from our MD simulations of 160 000 particles and 7000 independent configurations are $(6.869\pm 0.005)\beta^{-1}$ and $(25.51\pm 0.1)\beta^{-2}$. These are in excellent agreement with our theoretical results; the agreement in all other quantities shown below is of similar quality. Finally, the nth cumulant of χ is given by $(1/2)(n-1)!\sum_j(2\sigma_j)^n$.

Having looked at the distributions of local strain $\mathbf{e}$ and nonaffinity χ separately, we finally ask about their correlations. One can verify that, though small, the commutator $[\mathsf{P},\mathsf{C}]$ is nonvanishing, in contrast to the one-dimensional harmonic chain case. Indeed, measuring matrix sizes by the Euclidean norm $\|\mathsf{A}\| = \sqrt{\mathrm{Tr}\,\mathsf{AA}^t}$, we obtain for the chosen nearest-neighbor coarse-graining volume Ω

$$\begin{aligned}\beta\|\mathsf{C}\| = 3.875,\quad \beta\|[\mathsf{P},\mathsf{C}]\| = 0.124,\\ \beta\|[\mathsf{CP},[\mathsf{P},\mathsf{C}]]\| = 3.591\times 10^{-2}.\end{aligned} \tag{34}$$

Neglecting the commutator to first approximation gives a joint distribution of χ and $\mathbf{e}$ that factorizes into $P(\chi)$ and $P(\mathbf{e})$ without any correlation. The result of this calculation for the joint probability $P(\chi,e_1)$ is shown in Fig. 6(a). In actual fact, however, correlations are present. This means that the effective compliance of the solid depends on the value of χ (and vice versa). The effect is quantitatively rather small for our example system, as is clear from Fig. 6(b) where we plot the first correction to the factorized approximation. More simply, the coupling between χ and $\mathbf{e}$ can be assessed by looking at cross correlations like

$$\langle\chi\mathbf{e}\mathbf{e}^t\rangle - \langle\chi\rangle\langle\mathbf{e}\mathbf{e}^t\rangle = 2\mathsf{QC}[\mathsf{P},\mathsf{C}]\mathsf{Q}^t. \tag{35}$$

This result follows from the fact that the left-hand side is a third-order cumulant because $\langle\mathbf{e}\rangle = 0$, and so is proportional to the coefficient of the $O(k\kappa^2)$ term in the expansion (21) of $\ln\Phi(k,\kappa)$. The commutator $[\mathsf{P},\mathsf{C}]$ only appears linearly here; higher orders would be needed to express correlations

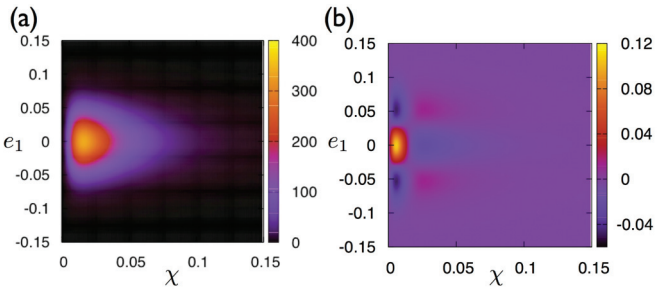

FIG. 6. (Color online) (a) Plot of $P(\chi,e_1) \approx P(\chi)P(e_1)$ as obtained from our calculations neglecting cross correlations and (b) the correction term $P(\chi,e_1) - P(\chi)P(e_1)$, both at $\beta = 200$. Note that the correction term is nonzero though small. The results from our simulations for $P(\chi,e_1)$ are indistinguishable from (a). The plots for other components of $\mathbf{e}$ are similar.

involving higher moments such as $\langle(\chi - \langle\chi\rangle)^n \mathbf{e}\mathbf{e}^t\rangle$. Using the numerically calculated $[\mathsf{P},\mathsf{C}]$ in (35) we obtain the following third-order cross correlation of χ with the eigendistortions:

$$\langle\chi e_v^2\rangle - \langle\chi\rangle\langle e_v^2\rangle = \langle\chi\omega^2\rangle - \langle\chi\rangle\langle\omega^2\rangle = 0, \tag{36}$$

$$\langle\chi e_u^2\rangle - \langle\chi\rangle\langle e_u^2\rangle = \langle\chi e_s^2\rangle - \langle\chi\rangle\langle e_s^2\rangle = 5.108 \times 10^{-3}\beta^{-2}. \tag{37}$$

One reads off that nonaffinity is coupled with uniaxial strain and shear strain, while local volume strain and rotational distortions do not generate nonaffinity. (This remains true also for correlations involving higher orders of χ.) The correlations of χ with e_u and e_s are positive, so that a large affine strain locally is generally accompanied by a large nonaffinity χ. Conversely, a large value of χ makes the local region more elastically compliant, i.e., typically leads to larger affine strains $\mathbf{e}$. More explicitly, the affine displacements $(\mathsf{I} - \mathsf{P})\mathbf{\Delta}$ conditional on the nonaffine ones $\mathsf{P}\mathbf{\Delta}$ can be written as a linear function of $\mathsf{P}\mathbf{\Delta}$ plus Gaussian fluctuations that do not depend on $\mathsf{P}\mathbf{\Delta}$. Thus one can find the distribution of the affine displacements, and hence of $\mathbf{e}$, conditional on χ from the distribution of the first contribution across all nonaffine displacements satisfying $(\mathsf{P}\mathbf{\Delta})^2 = \chi$. Because the first contribution is linear in Δ, one deduces that $\mathbf{e}$ is a sum of a random contribution proportional to $\chi^{1/2}$, and an independent Gaussian contribution. From this it follows, for example, that $\langle\chi^n \mathbf{e}\mathbf{e}^t\rangle = \langle\chi^{n+1}\rangle\mathbf{M}_1 + \langle\chi^n\rangle\mathbf{M}_2$, where $\mathbf{M}_1$ and $\mathbf{M}_2$ are two n-independent matrices related to C.

The strength of the coupling between χ and $\mathbf{e}$ will of course depend on the chosen coarse-graining region Ω, and in particular, on its radius R_Ω; we return to this topic in Sec. VI. But we believe that the positive correlation between the strengths of local affine and nonaffine deformations is not specific to the harmonic system considered here and should hold generally for all solids.

IV. TWO-POINT DISTRIBUTIONS AND CORRELATION FUNCTIONS

We now turn our attention to the spatial correlations of χ and $\mathbf{e}$. This requires us to consider simultaneously the displacement differences in *two* neighborhoods Ω and $\bar{\Omega}$ centered on lattice

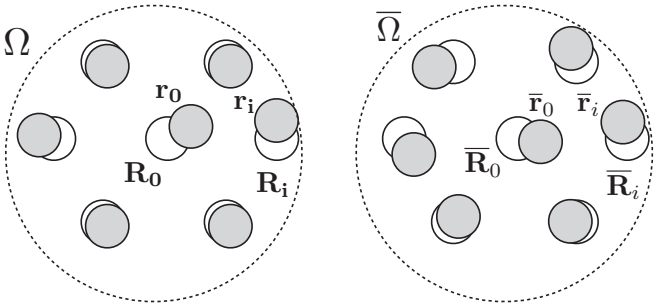

FIG. 7. Typical neighborhoods Ω and $\bar{\Omega}$ around particles 0 and $\bar{0}$ in the $d = 2$ triangular lattice, illustrating the definitions used for obtaining the two-point correlation functions. The labels have the same meanings as in Fig. 2.

positions $\mathbf{R}_0$ and $\bar{\mathbf{R}}_0$, respectively. The vector $\mathbf{\Delta}$ is defined as above, with an analogous definition for $\bar{\mathbf{\Delta}}$. The geometry and notation for the $d = 2$ triangular lattice are given in Fig. 7; the $d = 1$ case is straightforward. The local affine strain $\mathbf{e} = \mathsf{Q}\mathbf{\Delta}$ and nonaffinity $\chi = \mathbf{\Delta}^t\mathsf{P}\mathbf{\Delta}$ around $\mathbf{R}_0$ are then as before for Ω, whereas for $\bar{\Omega}$ we have the corresponding quantities $\bar{\mathbf{e}} = \bar{\mathsf{Q}}\bar{\mathbf{\Delta}}$ and $\bar{\chi} = \bar{\mathbf{\Delta}}^t\bar{\mathsf{P}}\bar{\mathbf{\Delta}}$. Note that since the reference $\bar{\Omega}$ is just a translated copy of Ω, one has $\bar{\mathsf{Q}} = \mathsf{Q}$ and $\bar{\mathsf{P}} = \mathsf{P}$.

To obtain the joint distribution of χ, $\mathbf{e}$, $\bar{\chi}$, and $\bar{\mathbf{e}}$ we need the joint Gaussian distribution of the displacements $\mathbf{\Delta}$ and $\bar{\mathbf{\Delta}}$. These have covariances

$$\begin{aligned} C_{i\alpha,j\gamma} &= \langle\Delta_{i\alpha}\Delta_{j\gamma}\rangle, \quad \bar{C}_{i\alpha,j\gamma} = \langle\bar{\Delta}_{i\alpha}\bar{\Delta}_{j\gamma}\rangle, \\ \tilde{C}_{i\alpha,j\gamma} &= \langle\Delta_{i\alpha}\bar{\Delta}_{j\gamma}\rangle. \end{aligned} \tag{38}$$

While the first two averages are identical, corresponding to two different but equivalent lattice sites, the third quantity encodes the displacement correlations between the two different sites. It may be obtained from an expression similar to (13),

$$\tilde{C}_{i\alpha,j\gamma} = l^2 \int \frac{d\mathbf{q}}{v_{\mathrm{BZ}}} \tilde{\mathcal{D}}^{-1}_{\alpha\gamma}(\mathbf{q})(e^{i\mathbf{q}\cdot\mathbf{R}_i} - e^{i\mathbf{q}\cdot\mathbf{R}_0})(e^{-i\mathbf{q}\cdot\bar{\mathbf{R}}_j} - e^{-i\mathbf{q}\cdot\bar{\mathbf{R}}_0}). \tag{39}$$

Note that $\tilde{C}_{i\alpha,j\gamma}$ is not symmetric with respect to interchanging $\mathbf{R}_0$ and $\bar{\mathbf{R}}_0$, although the correlation functions obtained from it below are, as they must be.

We could now proceed as for the local distribution $P(\chi,\mathbf{e})$ and derive the characteristic function $\Phi(k,\boldsymbol{\kappa},\bar{k},\bar{\boldsymbol{\kappa}})$ of the joint distribution $P(\chi,\mathbf{e},\bar{\chi},\bar{\mathbf{e}})$. This contains rather too much information to present in a concise manner, however, so we focus directly on the correlation functions. The simplest one of these is the strain-strain correlator

$$\langle\mathbf{e}\bar{\mathbf{e}}^t\rangle = \langle\mathsf{Q}\mathbf{\Delta}\bar{\mathbf{\Delta}}^t\mathsf{Q}^t\rangle = \mathsf{Q}\tilde{\mathsf{C}}\mathsf{Q}^t \tag{40}$$

In order to obtain space dependent correlation functions, this quantity needs to be evaluated for all choices of $\bar{\mathbf{R}}_0$ for fixed $\mathbf{R}_0$ (which may again be taken as the origin).

Alternatively, one may obtain the correlation functions in $\mathbf{q}$ space. As a side effect, this avoids the Brillouin zone integration in (39). To see this, write

$$\begin{aligned} \tilde{C}_{i\alpha,j\gamma} = l^2 \int \frac{d\mathbf{q}}{v_{\mathrm{BZ}}} \tilde{\mathcal{D}}^{-1}_{\alpha\gamma}(\mathbf{q})(e^{i\mathbf{q}\cdot(\mathbf{R}_i-\mathbf{R}_0)} - 1) \\ \times(e^{-i\mathbf{q}\cdot(\bar{\mathbf{R}}_j-\bar{\mathbf{R}}_0)} - 1)e^{i\mathbf{q}\cdot(\mathbf{R}_0-\bar{\mathbf{R}}_0)}. \end{aligned} \tag{41}$$

Now because the reference positions in Ω and $\bar{\Omega}$ are just translated copies of each other, one has $\bar{\mathbf{R}}_j - \bar{\mathbf{R}}_0 = \mathbf{R}_j - \mathbf{R}_0$, so that the only $\bar{\mathbf{R}}_0$ dependence resides in the last factor. Defining the Fourier transform of $\bar{C}_{i\alpha,j\gamma}$ via $\bar{C}_{i\alpha,j\gamma} = l^2 v_{\mathrm{BZ}}^{-1} \int d\mathbf{q}\, \tilde{C}_{i\alpha,j\gamma}(\mathbf{q}) e^{i\mathbf{q}\cdot(\mathbf{R}_0 - \bar{\mathbf{R}}_0)}$ one thus reads off

$$\bar{C}_{i\alpha,j\gamma}(\mathbf{q}) = \tilde{\mathcal{D}}^{-1}_{\alpha\gamma}(\mathbf{q})(e^{i\mathbf{q}\cdot(\mathbf{R}_i - \mathbf{R}_0)} - 1)(e^{-i\mathbf{q}\cdot(\bar{\mathbf{R}}_j - \bar{\mathbf{R}}_0)} - 1). \tag{42}$$

The Fourier transform of the strain correlation functions is then simply

$$\langle \mathbf{e}\bar{\mathbf{e}}^t \rangle(\mathbf{q}) = \mathsf{Q}\bar{\mathsf{C}}(\mathbf{q})\mathsf{Q}^{\mathbf{t}} \tag{43}$$

and can be written down in closed form provided the dynamical matrix $\tilde{\mathcal{D}}(\mathbf{q})$ for the lattice is known.

Next we consider the spatial correlation functions of the nonaffinity, $\langle \chi\bar{\chi}\rangle - \langle\chi\rangle\langle\bar{\chi}\rangle$. It is convenient, at this stage, to define the vectors $\mathbf{Y} = \mathsf{P}\boldsymbol{\Delta}$ and $\bar{\mathbf{Y}} = \mathsf{P}\bar{\boldsymbol{\Delta}}$ with components y_j and $\bar{y}_j$, where $j = 1, \ldots, Nd$. Thus $\chi = \sum_{j=1}^{Nd} y_j^2$ and $\chi\bar{\chi} = \sum_{i,j=1}^{Nd} y_i^2 \bar{y}_j^2$. Hence the correlation between χ and $\bar{\chi}$ is given by

$$\begin{aligned}\langle \chi\bar{\chi}\rangle - \langle\chi\rangle\langle\bar{\chi}\rangle &= \sum_{i,j=1}^{Nd} \left(\langle y_i^2 \bar{y}_j^2\rangle - \langle y_i^2\rangle\langle\bar{y}_j^2\rangle\right) \\ &= 2\sum_{i,j=1}^{Nd} \langle y_i \bar{y}_j\rangle^2 \;=\; 2\sum_{i,j=1}^{Nd} (\mathsf{P}\bar{\mathsf{C}}\mathsf{P})_{ij}^2 \\ &= 2\,\mathrm{Tr}(\mathsf{P}\bar{\mathsf{C}}\mathsf{P})(\mathsf{P}\bar{\mathsf{C}}\mathsf{P})^t \end{aligned} \tag{44}$$

using Wick's theorem. If in line with our earlier notation we use $\bar{\sigma}_j^2$ to denote the Nd eigenvalues of the matrix $(\mathsf{P}\bar{\mathsf{C}}\mathsf{P})(\mathsf{P}\bar{\mathsf{C}}\mathsf{P})^t$, then the last expression can be simplified to

$$\langle \chi\bar{\chi}\rangle - \langle\chi\rangle^2 = 2\sum_{j=1}^{Nd} \bar{\sigma}_j^2. \tag{45}$$

Note that if $\mathsf{P}\bar{\mathsf{C}}\mathsf{P}$ itself happens to be symmetric, then the $\bar{\sigma}_j^2$ can be obtained as the squares of the eigenvalues of this matrix. As for the real-space strain correlator, one has to evaluate (45) for different choices of $\bar{\mathbf{R}}_0$ to obtain spatial profiles of the nonaffinity correlator.

Finally one could ask about spatial cross correlations like $\langle \chi\bar{\mathbf{e}}\bar{\mathbf{e}}^t\rangle - \langle\chi\rangle\langle\bar{\mathbf{e}}\bar{\mathbf{e}}^t\rangle$. We do not pursue this here: As we saw above, these correlations are already rather weak (at least for coarse graining across nearest neighbors) locally, i.e., when $\mathbf{R}_0 = \bar{\mathbf{R}}_0$.

A. The one-dimensional harmonic chain

We now apply the above framework to the one-dimensional harmonic chain introduced in Sec. III A. We choose as the first reference location $x_0 = 0$ and as the second $\bar{x}_0 = ml$. Coarse graining will be across the nearest neighbors $x_{\pm 1}$ in Ω and $\bar{x}_{\pm 1} = (m \pm 1)l$ in $\bar{\Omega}$. The matrix $\bar{C}_{jk}$ is then given by

$$\bar{C}_{jk} = l^2 \int_0^{2\pi/l} \frac{dq}{2\pi/l} \frac{F(q)}{\tilde{\mathcal{D}}(q)}, \tag{46}$$

where

$$\begin{aligned} F(q) &= (e^{iq\,x_j} - 1)(e^{-iq\,\bar{x}_k} - e^{-iq\,\bar{x}_0}) \\ &= e^{-iq\bar{x}_0}(e^{iq(j-k)l} - e^{iqjl} - e^{-iqkl} + 1). \end{aligned} \tag{47}$$

There are now two possibilities. If $j = k$ then, bearing in mind that $\tilde{\mathcal{D}}(q) = 2\beta[1 - \cos(ql)]$, one has $F(q)/\tilde{\mathcal{D}}(q) = \beta^{-1} e^{-iq\bar{x}_0}$ so that $\bar{C}_{jk} = 0$ except when $\bar{x}_0 = 0$. Otherwise, if $j = -k$, then $F(q)/D(q) = -\beta^{-1} e^{iq(jl - \bar{x}_0)}$ so that now $\bar{C}_{jk} = 0$ unless $\bar{x}_0 = jl$. For all other cases, $\bar{C}_{jk}$ vanishes identically. Summarizing, $\bar{\mathsf{C}}$ equals C from (23) when $\bar{x}_0 = 0 = x_0$; for $\bar{x}_0 = l$ it is given by

$$\bar{\mathsf{C}} = l^2\beta^{-1} \begin{pmatrix} 0 & -1 \\ 0 & 0 \end{pmatrix}, \tag{48}$$

while for $\bar{x}_0 = -l$ one obtains the transpose. For all larger distances $|\bar{x}_0| \geqslant 2l$, $\bar{\mathsf{C}} = 0$, indicating that χ and ϵ are uncorrelated beyond nearest neighbors. The intuition here is as discussed after (23), namely that the relative particle displacements of all nearest neighbor pairs fluctuate independently from each other. Accordingly, the single nonzero entry in (48) comes from the correlation of the displacements $u_1 = x_1 - x_0$ and $\bar{u}_{-1} = \bar{x}_{-1} - \bar{x}_0 = x_0 - x_1$, and so is simply the negative variance of u_1.

To obtain the correlation functions we need the matrices $\mathsf{P}\bar{\mathsf{C}}\mathsf{P}^t$ and $\mathsf{Q}\bar{\mathsf{C}}\mathsf{Q}^t$, where we can focus directly on the only nonzero correlations at $\bar{x}_0 = \pm l$. Even though $\bar{\mathsf{C}}$ is then not symmetric, $\mathsf{P}\bar{\mathsf{C}}\mathsf{P}^t$ is, and has eigenvalues $\bar{\sigma} = \frac{1}{2}l^2\beta^{-1}$ and 0. On the other hand, the scalar $\mathsf{Q}\bar{\mathsf{C}}\mathsf{Q}^t$ equals $\frac{1}{4}\beta^{-1}$. Using (45), the correlation functions $\langle\chi(0)\chi(ml)\rangle - \langle\chi\rangle^2$ and $\langle\epsilon(0)\epsilon(ml)\rangle$ can then be written as follows:

$$\begin{aligned} \langle\chi(0)\chi(ml)\rangle - \langle\chi\rangle^2 &= 2\sigma^2 = 2l^4\beta^{-2}, \quad m = 0 \\ &= 2\bar{\sigma}^2 = \tfrac{1}{2}\,l^4\beta^{-2}, \quad m = \pm 1 \\ &= 0, \quad |m| \geqslant 2, \\ \langle\epsilon(0)\epsilon(m\,l)\rangle &= \tfrac{1}{2}\beta^{-1}, \quad m = 0 \\ &= \tfrac{1}{4}\beta^{-1}, \quad m = \pm 1 \\ &= 0, \quad |m| \geqslant 2. \end{aligned}$$

As expected the correlation functions, being symmetric, depend only on the magnitude and not on the direction of $\bar{x}_0 = ml$.

Summarizing, the correlation functions for χ and ϵ in $d = 1$ are always short ranged, vanishing identically beyond the nearest neighbor. Correlation functions in the two-dimensional lattice have much more structure as we will see next.

B. The two-dimensional harmonic triangular net

The calculation of the correlation function for the two-dimensional triangular lattice follows along lines similar to that of the single-point distribution functions, except that results now have to be obtained for each lattice position $\bar{\mathbf{R}}_0$. For the χ correlations, we calculate the trace of $(\mathsf{P}\bar{\mathsf{C}}\mathsf{P})(\mathsf{P}\bar{\mathsf{C}}\mathsf{P})^t$ as the sum of the 12 eigenvalues $\bar{\sigma}_j^2$ and use (45) to find $\langle\chi(\mathbf{0})\chi(\mathbf{R})\rangle - \langle\chi\rangle^2$, where $\mathbf{R} = \bar{\mathbf{R}}_0 - \mathbf{R}_0$. The results obtained using this calculation are compared with simulations in Fig. 8,

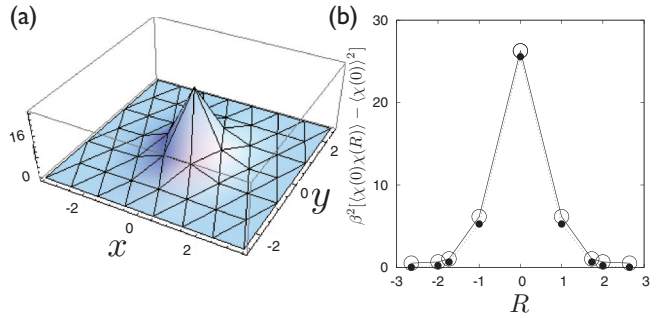

FIG. 8. (Color online) (a) Surface plot of $\beta^2(\langle\chi(\mathbf{0})\chi(\mathbf{R})\rangle - \langle\chi\rangle^2)$ over the two-dimensional triangular lattice from our exact calculation. (b) Quantitative comparison for the orientation averaged $\beta^2(\langle\chi(0)\chi(R)\rangle - \langle\chi\rangle^2)$, where $R = |\bar{\mathbf{R}}_0 - \mathbf{R}_0|$. Open circles show the values obtained from our exact calculation and filled circles those from simulations of a 100×100 particle system. The solid lines are guides to the eye.

showing that this function is isotropic and decays within about two to three lattice spacings, similar to the results obtained in Refs. [17,18].

Similarly the spatial correlation function for the strain may be obtained by evaluating $\langle \mathbf{e}\bar{\mathbf{e}}^t\rangle = \langle \mathbf{Q}\mathbf{\Delta}\bar{\mathbf{\Delta}}^t\mathbf{Q}^t\rangle = \mathbf{Q}\bar{\mathbf{C}}\mathbf{Q}^t$ for a range of spatial separations $\mathbf{R}$. The results are shown in Fig. 9. The correlation functions of e_v and ω decay rapidly to zero and are nearly isotropic. We take advantage of this approximate symmetry by averaging over all pairs $(\mathbf{R}_0, \bar{\mathbf{R}}_0)$ related by symmetry to produce angle-averaged correlation functions that are functions of $R = |\bar{\mathbf{R}}_0 - \mathbf{R}_0|$ alone. Results for these functions are compared with those obtained from simulations in Fig. 10(a). Correlations involving the uniaxial (e_u) and shear

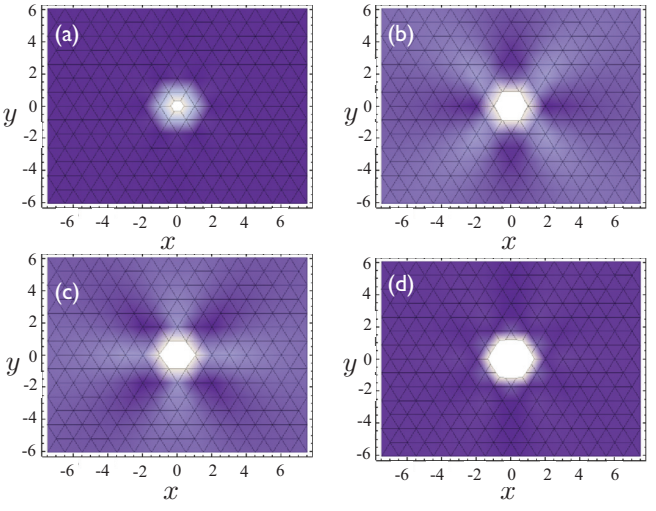

FIG. 9. (Color online) Density plot of the correlation functions as obtained from our calculations showing the shape of the correlation functions in the two-dimensional plane (a) $\beta\langle e_v(\mathbf{0})e_v(\mathbf{R})\rangle$, (b) $\beta\langle e_u(\mathbf{0})e_u(\mathbf{R})\rangle$, (c) $\beta\langle e_s(\mathbf{0})e_s(\mathbf{R})\rangle$, and (d) $\beta\langle\omega(\mathbf{0})\omega(\mathbf{R})\rangle$. Note that the volume and rotational correlations are nearly isotropic, while the uniaxial and shear strain correlations show fourfold anisotropy. The colors vary from dark blue (dark gray) (-0.1) to white (0.2) for all the plots. To keep a uniform scale for all graphs we have a cut off for the large values at the origin.

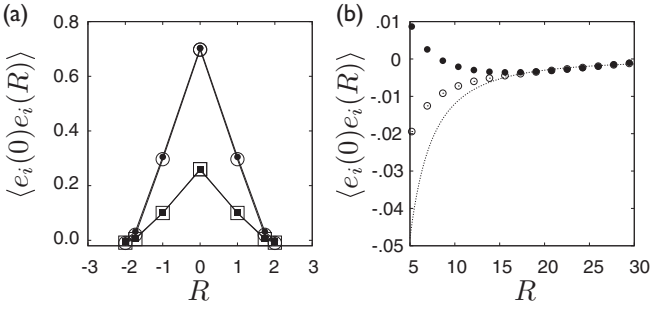

FIG. 10. (a) Quantitative comparison for the (orientation averaged) volume and rotational deformation correlations $\beta\langle e_v(0)e_v(R)\rangle$ (squares) and $\beta\langle\omega(0)\omega(R)\rangle$ (circles). The open symbols are from our exact calculations and the filled ones are from our simulations of the 100×100 particle system. The solid lines are guides to the eye. The agreement in the numerical values for the correlations for other components of the distortion tensor are similar. (b) The large length scale behavior of $\beta\langle e_u(0,0)e_u(R/\sqrt{2}, R/\sqrt{2})\rangle$ (open circles) and $\beta\langle e_s(0,0)e_s(0,R)\rangle$ (filled circles) showing the slow decay along these directions. The dotted line shows the $\sim R^{-2}$ behavior for comparison.

(e_s) strains exhibit a pronounced fourfold anisotropy at large distances, with prominent lobes at 0, π, $\pm\pi/2$, $\pm\pi/4$, and $\pm 3\pi/4$. Furthermore, $\langle e_u(\mathbf{0})e_u(\mathbf{R})\rangle$ and $\langle e_s(\mathbf{0})e_s(\mathbf{R})\rangle$ appear to be rotated by $\pi/4$ with respect to one another [see Figs. 9(b) and 9(c)] for large $|\mathbf{R}|$. At small distances, of course, this correspondence is not exactly satisfied because the underlying triangular lattice does not have this $\pi/4$ rotational symmetry.

An identical $\pi/4$ anisotropy is also observed in momentum space (Fig. 11) where one can obtain closed form expressions for the correlation functions, in particular, in the $\mathbf{q} \to 0$ limit as we show below. We begin by writing down explicit expressions for the strain correlation functions in component form. With

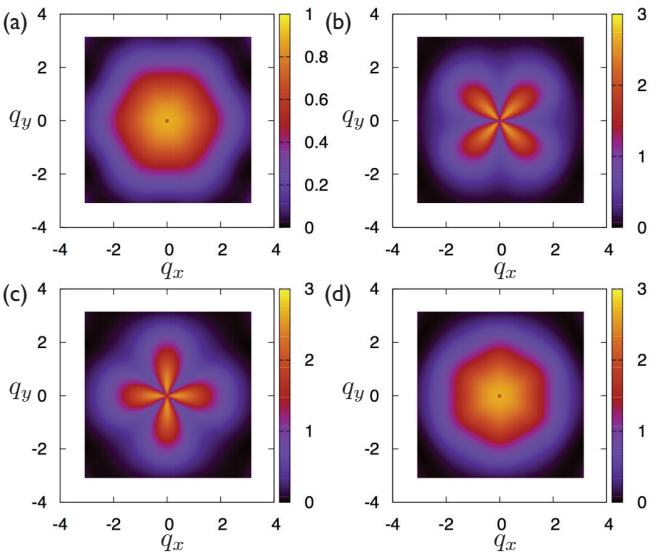

FIG. 11. (Color online) Plot of the correlation functions in $\mathbf{q}$ space obtained from (42). (a) $\langle e_v^2\rangle(\mathbf{q})$, (b) $\langle e_u^2\rangle(\mathbf{q})$, (c) $\langle e_s^2\rangle(\mathbf{q})$, and (d) $\langle\omega^2\rangle(\mathbf{q})$. The key to the color values is given beside each plot. Note the fourfold symmetry of the uniaxial and shear correlations similar to the real-space plots shown in Fig. 9.

the abbreviation $\mathsf{E} = \mathsf{Q}\bar{\mathsf{C}}(\mathbf{q})\mathsf{Q}^t$ one has

$$\begin{aligned}\langle e_v^2\rangle(\mathbf{q}) &= \mathsf{E}_{1111} + \mathsf{E}_{2222} + 2\mathsf{E}_{1122},\\ \langle e_u^2\rangle(\mathbf{q}) &= \mathsf{E}_{1111} + \mathsf{E}_{2222} - 2\mathsf{E}_{1122},\\ \langle e_s^2\rangle(\mathbf{q}) &= \mathsf{E}_{1212} + \mathsf{E}_{2121} + 2\mathsf{E}_{1221},\\ \langle \omega^2\rangle(\mathbf{q}) &= \mathsf{E}_{1212} + \mathsf{E}_{2121} - 2\mathsf{E}_{1221}.\end{aligned} \tag{49}$$

The notation used here is the same as in (43), so that, e.g., $\langle e_v^2\rangle(\mathbf{q})$ is the Fourier transform of the strain correlator $\langle e_v \bar{e}_v\rangle \equiv \langle e_v(\mathbf{R}_0) e_v(\bar{\mathbf{R}}_0)\rangle = v_{\mathrm{BZ}}^{-1}\int d\mathbf{q}\,\langle e_v^2(\mathbf{q})\rangle e^{i\mathbf{q}\cdot(\mathbf{R}_0-\bar{\mathbf{R}}_0)}$. After substituting in for $\bar{\mathsf{C}}(\mathbf{q})$ from (42) one gets, using also that for the triangular lattice $\mathsf{R}^t\mathsf{R}$ is three times the identity matrix,

$$\mathsf{E}_{\alpha\alpha'\gamma\gamma'} = \frac{1}{9}\sum_{i,j=1}^{6} f^{ij} R_{i\alpha'} R_{j\gamma'} \tilde{\mathcal{D}}^{-1}_{\alpha\gamma}(\mathbf{q}) \tag{50}$$

with

$$\begin{aligned} f^{ij} &= f_R^{ij} + i f_I^{ij},\\ f_R^{ij} &= \cos[\mathbf{q}\cdot(\mathbf{R}_i - \mathbf{R}_j)] - \cos(\mathbf{q}\cdot\mathbf{R}_i) - \cos(\mathbf{q}\cdot\mathbf{R}_j) + 1,\\ f_I^{ij} &= \sin[\mathbf{q}\cdot(\mathbf{R}_m - \mathbf{R}_n)] - \sin(\mathbf{q}\cdot\mathbf{R}_i) + \sin(\mathbf{q}\cdot\mathbf{R}_j). \end{aligned} \tag{51}$$

Noting that the imaginary contributions to E sum to zero and expanding f_R^{ij} in Eq. (50) yields for small q,

$$\begin{aligned}\mathsf{E}_{\alpha\alpha'\gamma\gamma'} &= \frac{1}{9}\sum_{i,j=1}^{6}\sum_{\mu\nu} q_\mu q_\nu R_{i\mu} R_{j\nu} R_{i\alpha'} R_{j\gamma'} \tilde{\mathcal{D}}^{-1}_{\alpha\gamma}(\mathbf{q})\\ &= q_{\alpha'} q_{\gamma'} \tilde{\mathcal{D}}^{-1}_{\alpha\gamma}(\mathbf{q}),\end{aligned} \tag{52}$$

where we have used again that $\sum_i R_{i\alpha} R_{i\gamma} = 3\delta_{\alpha\gamma}$. To examine the leading order behavior at small $\mathbf{q}$ for the strain correlators, we expand $\mathcal{D}^{-1}(\mathbf{q})$ about $\mathbf{q} = 0$ in (52) and substitute into (49) to obtain

$$\langle e_v^2\rangle(\mathbf{q}) \approx \frac{8}{9}, \tag{53}$$

$$\langle e_u^2\rangle(\mathbf{q}) \approx \frac{8}{9} + \frac{64}{9}\frac{q_x^2 q_y^2}{\left(q_x^2+q_y^2\right)^2}, \tag{54}$$

$$\langle e_s^2\rangle(\mathbf{q}) \approx \frac{8}{3} - \frac{64}{9}\frac{q_x^2 q_y^2}{\left(q_x^2+q_y^2\right)^2}, \tag{55}$$

$$\langle \omega^2\rangle(\mathbf{q}) \approx \frac{8}{3} \tag{56}$$

consistent with the results plotted in Fig. 11. The fact that the correlators of uniaxial strain e_u and shear strain e_s are related by a rotation becomes clearer if one rewrites (55) as

$$\langle e_s^2(\mathbf{q})\rangle \approx \frac{8}{9} + \frac{64}{9\left(q_x^2+q_y^2\right)^2}\left[\left(\frac{q_x+q_y}{\sqrt{2}}\right)^2\left(\frac{q_x-q_y}{\sqrt{2}}\right)^2\right]. \tag{57}$$

This evidently maps to (54) under a rotation by $\pi/4$, as claimed. We note that the large distance (small $\mathbf{q}$) anisotropies of $\langle e_u^2(\mathbf{q})\rangle$ and $\langle e_s^2(\mathbf{q})\rangle$ are also consistent with a mean field, continuum theory calculation shown in detail in Ref. [18]. Interestingly, that calculation restricted attention to fluctuating strain fields that satisfy force balance, so one concludes that it is indeed these configurations that dominate the scaling for large distances.

The $\mathbf{q}$-space structure of the uniaxial and the shear correlation functions as implied by (56), Figs. 11(b) and 11(c), and further supported by continuum theory [18], shows that these correlation functions have singularities at $q = 0$, with the second terms in (54) and (57) vanishing along specific directions ($q_x = 0$, $q_y = 0$ in e_u and $q_x = \pm q_y$ in e_s). These singularities lead to slow ($\sim 1/R^2$) decay of the correlation functions in real space [see Fig. 10(b)], with the prefactor alternating in sign according to $\cos(4\theta)$ or $\sin(4\theta)$ with the polar angle of $\mathbf{R}$.

Before we end this section, we remark that the strain correlation functions, by linear response, are proportional to the strain field produced by a point, delta function stress at the origin. Since the large R (or small q) structure of the correlation functions is insensitive to crystal symmetry, it is no surprise that similar quadrupolar displacement patterns [28] have been observed in association with local rearrangements in amorphous materials known as shear transformation zones (STZ) [7,8,29], in both experiments [30] and computer simulations [31,32] of granular or glassy materials under shear.

V. LINEAR RESPONSE AND THE NONAFFINE FIELD

The form of the characteristic function (15) offers a simple way to calculate the response of the system to uniform fields conjugate to χ and $\mathbf{e}$. We analytically continue k and $\boldsymbol{\kappa}$ to the complex plane by replacing $\boldsymbol{\kappa} \to \boldsymbol{\kappa} - i\,\boldsymbol{\Sigma}$ and $k \to k - i\,h_\chi$. Here the vector $\boldsymbol{\Sigma}$, once rearranged into a symmetric tensor, is the stress [9], made dimensionless by multiplying by the inverse temperature β and the size of a suitable local volume of the order of R_Ω^d. On the other hand, h_χ is a new field, conjugate to χ. The introduction of a (small) stress merely shifts $\langle\mathbf{e}\rangle$ away from zero to a value proportional to Σ (Hooke's law), i.e., $\langle e_i\rangle_{\boldsymbol{\Sigma}} = \langle e_i e_j\rangle_{\boldsymbol{\Sigma}=0}\Sigma_j$. The proportionality constant here is the zero field compliance calculated earlier. Furthermore, because of the coupling between $\mathbf{e}$ and χ, external stress [mainly shear and uniaxial; see Sec. III and Eq. (36)] will change $P(\chi)$ for lattices where [P,C] and higher commutators are nonzero. A straightforward calculation, introducing $\boldsymbol{\Sigma}$ in (21) and Taylor expanding, shows that for small values of $\boldsymbol{\Sigma}$,

$$\langle\chi\rangle_{\boldsymbol{\Sigma}} = \langle\chi\rangle_{\boldsymbol{\Sigma}=0} + \boldsymbol{\Sigma}^t\mathsf{QC}[\mathsf{P},\mathsf{C}]\mathsf{Q}^t\boldsymbol{\Sigma}, \tag{58}$$

which always increases $\langle\chi\rangle$ for the $d = 2$ triangular lattice; higher moments of χ are similarly affected. A similar dependence on external stress for nonaffinity arising from quenched disorder has been discussed in Ref. [12]. Unlike in Ref. [12], however, the contribution of (58) is, in addition, proportional to T^2. At large $\boldsymbol{\Sigma}$, of course, perturbations would become so large that the effects of anharmonicities that we have not modeled would become apparent causing, finally, the nucleation of defects.

The effect of h_χ is also intriguing. Below we illustrate this explicitly for the one-dimensional case, though similar results should hold in any dimension and for particles with arbitrary interactions. The joint characteristic function for χ and e for

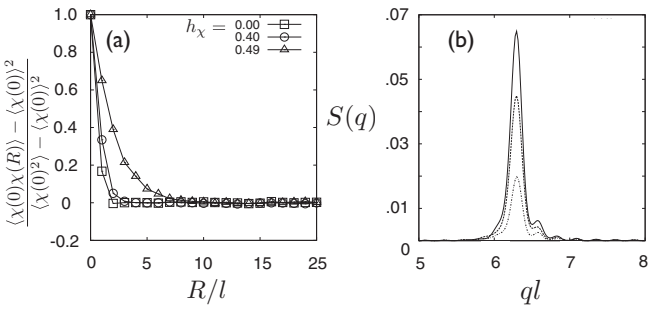

FIG. 12. (a) The scaled, two-point χ-χ correlation function for $h_\chi = 0$, 0.4, and 0.49 from Monte Carlo simulations of a 50 particle harmonic chain at $\beta = 100$, showing a large increase in the correlation length as the critical field is approached. (b) The first peak in the structure factor $S(q) = \langle \rho_q \rho_{-q} \rangle$ for $h_\chi = 0$ (solid line), 0.4 (dashed line), and 0.49 (dash-dotted line) for the same system as in (a). Note that the amount of structure is reduced at constant temperature.

the $d = 1$ chain with h_χ included is

$$\Phi(k,\kappa) = \sqrt{\frac{1 - 2\sigma h_\chi}{1 - 2\sigma i k - 2\sigma h_\chi}} \exp\left(-\frac{1}{2}\langle\epsilon^2\rangle\kappa^2\right). \quad (59)$$

Note that we have multiplied $\Phi(k,\kappa)$ by the factor $\sqrt{1 - 2\sigma h_\chi}$ to ensure normalization, i.e., $\lim_{k\to 0,\kappa\to 0}\Phi(k,\kappa) = 1$. Now we can obtain $P(\epsilon)$, $P(\chi)$, and $P(\chi,\epsilon)$ by inspection as

$$\begin{aligned} P(\chi,\epsilon) &= P(\chi)P(\epsilon) \\ &= \sqrt{\frac{1 - 2\sigma h_\chi}{2\pi\sigma}}\chi^{-1/2}\exp\left[-\frac{(1 - 2\sigma h_\chi)\chi}{2\sigma}\right] \\ &\quad \times \frac{1}{\sqrt{2\pi\langle\epsilon^2\rangle}}\exp\left[-\frac{\epsilon^2}{2\langle\epsilon^2\rangle}\right]. \end{aligned} \quad (60)$$

As $h_\chi \to 1/(2\sigma)$, $P(\chi)$ becomes proportional to $\chi^{-1/2}$ and all the moments

$$\langle\chi^n\rangle = \left(\frac{2\sigma}{1 - 2\sigma h_\chi}\right)^n \frac{\Gamma\left(n + \frac{1}{2}\right)}{\Gamma\left(\frac{1}{2}\right)}$$

diverge as $[h_\chi - 1/(2\sigma)]^{-n}$. Spatial correlations of nonaffinity χ also become long ranged in this limit and the system becomes disordered. Displacements acquire a nonaffine character over all length scales, as evidenced from the decrease of the amplitude of the structure factor for a finite one-dimensional chain of 50 particles [see Figs. 12(a) and 12(b)].

All of this suggests the presence of a critical line in the (h_χ,β) plane beyond which the system becomes globally nonaffine so that χ defined by coarse graining over local neighborhoods Ω is always infinite—a "maximally nonaffine" solid (the presence of anharmonicities would, in practice, be expected to limit χ to a finite value). For the $d = 1$ lattice, this transition is identical to the celebrated Peierls transition [25] as can be deduced from the nature of the nonaffine mode shown in Fig. 1(c). In higher dimensions, the transition appears for values of h_χ equal to a critical h_χ^* close to half the reciprocal of the largest eigenvalue of PCP^t. Indeed, one finds easily by writing down the general analog of (59), taking a log and differentiating with respect to ik that

$$\langle\chi\rangle = \mathrm{Tr}(\mathsf{I} - 2h_\chi\mathsf{PCP}^t)^{-1}, \quad (61)$$

which diverges at $h_\chi^* = 1/(2\max_j \sigma_j)$ if the σ_j are the eigenvalues of PCP^t as before. In the triangular net, the largest eigenvalues are $\sigma_1 = \sigma_2$ and the displacement patterns whose amplitudes would grow at the transition are shown in Figs. 3(a) and 3(b). Locally, they correspond to an almost uniform translation of the neighboring particles relative to the central particle, though it is difficult to visualize what global configuration is finally produced. We imagine that this leads to destruction of the lattice structure and eventual amorphization. Of course, as the transition is approached, we expect the identity of the neighborhoods, Ω, itself to become ill defined due to this loss of crystalline order, making many of our results invalid in that limit.

In the harmonic lattice, the transition discussed above is *hidden* because the only physically realizable value of the nonaffine field $h_\chi = 0$ lies on the critical line at infinite temperature $\beta = 0$. Nevertheless, there may be systems where the critical line cuts the $h_\chi = 0$ axis at a nonzero value of β (i.e., at finite temperature). In such a system one may obtain a physical transition from an affine to a maximally nonaffine state as the temperature is increased or a stiffness parameter is reduced producing a going over to a "glass spinodal" [33]. We speculate that this may also happen at or near the yield point of a solid under external load where the bonds between atoms become weak due to strong anharmonicities. However, for such cases, the simple linear response calculations presented above become invalid and the distributions of χ and $\mathbf{e}$ become strongly coupled through the strain and nonaffinity dependence of the dynamical matrix $\tilde{\mathcal{D}}(\mathbf{q})$. Implications of this transition for the mechanical and phase behavior of solids in one, two, and three dimensions are being worked out and will be published elsewhere.

VI. SUMMARY AND CONCLUSIONS

In this paper we have shown that coarse graining of the microscopic displacements of crystalline solid at nonzero temperatures generates nonaffine as well as locally affine distortions. The procedure effectively amounts to integrating out phonon modes with wavelengths comparable to or smaller than the coarse-graining length. We have obtained the probability distributions for the nonaffine parameter and the affine distortions of a harmonic lattice at nonzero temperatures. We have also obtained the spatial correlations of the local distortions and nonaffinity. While $\langle\chi(\mathbf{0})\chi(\mathbf{R})\rangle$ decays exponentially, the correlation functions corresponding to the different elements of the distortion tensor decay differently. Volume and rotation correlations, on the one hand, are short ranged; uniaxial and shear strain components, on the other hand, decay as a $1/R^2$ power law with prefactor depending on the polar angle as $\sin(4\theta)$ or $\cos(4\theta)$, respectively. The angular dependencies of the slow decay for uniaxial strain and shear are rotated by $\pi/4$ with respect to each other. We noted that this is consistent with an earlier continuum calculation imposing the mechanical stability condition that the stress is divergence free in the fluctuating strain field. Finally, we have shown that it is possible to induce a transition from a solid with a finite average nonaffinity $\langle\chi\rangle$ to one where all moments $\langle\chi^n\rangle$ diverge, by tuning a nonaffine field h_χ.

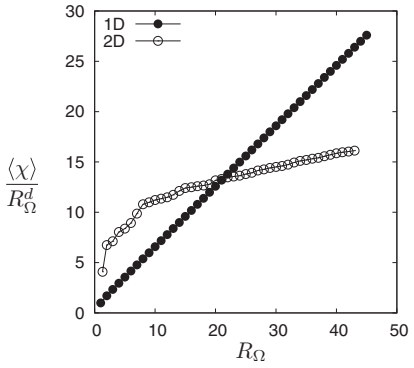

FIG. 13. Plot of $\langle\chi\rangle/R_\Omega^d$ vs R_Ω for $d = 1$ (filled circles) and $d = 2$ (open circles). Note that while the intensive (per unit coarse-graining volume) χ increases linearly with R_Ω, the size of the reference volume Ω, in $d = 1$, it has a much slower logarithmic increase in $d = 2$.

How do our results vary with the size of the reference volume Ω used to define the coarse-grained quantities? First, χ depends on the number of sites within Ω, so we need to consider the intensive quantity $\langle\chi\rangle/R_\Omega^d$, where R_Ω is the radius of the reference volume Ω. Furthermore, since χ depends on the fluctuations of the displacements $\mathbf{u}$, then in $d = 1$ this quantity itself should diverge as $\sim R_\Omega$ and in $d = 2$ as $\sim \log(R_\Omega)$ [10]. In Fig. 13 we show plots for this normalized nonaffinity in $d = 1$ and $d = 2$, which confirm these expectations. In higher dimensions the intensive variable $\langle\chi\rangle/R_\Omega^d$ should for large R_Ω approach a constant (proportional to temperature, as for $d = 1$ and 2). Note that the probability distribution of strains $P(\chi,\mathbf{e}_j)$ is similarly Ω dependent and so our calculation automatically incorporates exact finite size scaling of the elastic compliances. Approximate finite size scaling results based on continuum elasticity theory have been used to obtain elastic constants of colloidal solids from video microscopy data [16,17]. Our results may offer a better way to analyze such data.

Secondly, as R_Ω increases, χ and the distortion D may get more and more coupled. This is best illustrated, for the $d = 1$ harmonic chain, by computing the norms of the commutators $[\mathsf{P},\mathsf{C}]$ and $[\mathsf{CP},[\mathsf{P},\mathsf{C}]]$, which we obtain as shown in Table I.

TABLE I. Numerical values of the norm of the successive commutators of P and C which contribute to the cross correlation of nonaffinity and strain (see Sec. II). Note that the commutators increase with the size R_Ω of the reference volume.

R_Ω/l	$\|\mathsf{C}\|$	$\|[\mathsf{P},\mathsf{C}]\|$	$\|[\mathsf{CP},[\mathsf{P},\mathsf{C}]]\|$
1	1.414	0.000	0.000
2	3.741	0.282	0.126
3	7.211	0.654	0.534
4	11.832	1.148	1.516
5	17.606	1.766	3.448
6	24.535	2.507	6.803
7	32.619	3.371	12.145
8	41.856	4.358	20.132
9	52.249	5.469	31.520
10	63.796	6.704	47.154

For very large R_Ω more and more terms are needed to get good convergence of the Taylor expansion for $P(\chi,\mathbf{e}_j)$ in powers of k, viz., Eq. (21), for given k. Accordingly χ becomes inextricably linked with the strain, a phenomenon related to the fluctuation-driven instability of ordered solids in one dimension [10]. This effect should be weaker in higher dimensions, though a full study of the influence of dimensionality on nonaffinity for a variety of lattices and interactions needs further work.

Our calculations may be easily extended to other lattices and to higher dimensions without much difficulty, requiring at most a calculation of the relevant dynamical matrix. Similarly, local χ and displacement distributions can be obtained for crystals with isolated, point or line defects once the appropriate Hessians of the local potential energy at defects are evaluated. The effect of external stress on χ is another interesting problem which may be addressed immediately in the limit of negligible anharmonicity; the effect of anharmonic terms could be included perturbatively. Finally the effect of disorder can be incorporated [12] at nonzero temperatures.

Our results may also be used to construct new simulation strategies for investigating the mechanical behavior of solids under external stress. For instance, particle moves may be designed which change χ without influencing the local distortion within Ω by projecting particle displacements along eigendirections of P.

Such calculations will be particularly useful for glasses [7], where local potential energy Hessians may be used to define an equivalent harmonic lattice at every instance of time with χ being calculated dynamically from the reference configurations at the previous time step. Calculations similar to ours will be useful to understand the properties of STZ [29], defined [7,8] as regions with a large value of χ; these are the dominant entities responsible for mechanical deformation of glasses. STZ are thermally generated and respond to external stress by rearrangements of local particle positions. Similar localized nonaffine excitations have also been observed in anharmonic, crystalline solids [34] where they have been identified as droplet fluctuations from nearby glassy and liquidlike minima of the free energy. Constrained simulations like those outlined above may help in identifying the role of χ in the processes involved in complex phenomena such as anelasticity, yielding, and melting. The role of the nonaffine field h_χ in influencing glass transition and the mechanical behavior of solids both crystalline and amorphous is another direction that we intend to investigate in the future.

ACKNOWLEDGMENTS

S.G. and S.S. thank the DST India (Grant No. INT/EC/MONAMI/(28)233513/2008) for support. The present work was formulated during a visit by some of the authors (S.S., P.S., and M.R.) to the KITP Santa Barbara, where this research was supported in part by the National Science Foundation under Grant No. NSF PHY05-51164. S.G. thanks CSIR India for support through a Junior Research Fellowship. Discussions with Srikanth Sastry are gratefully acknowledged.

[1] *Soft and Fragile Matter: Nonequilibirum Dynamics, Metastability and Flow*, edited by M. Evans and M. Cates, The Scottish Universities Summer School in Physics Vol. 53 (Institute of Physics, London, 2000).

[2] F. C. MacKintosh, J. Käs, and P. A. Janmey, Phys. Rev. Lett. **75**, 4425 (1995); R. Everaers, Eur. Phys. J. B **4**, 341 (1998); J. U. Sommer and S. Lay, Macromolecules **35**, 9832 (2002); D. A. Head, F. C. MacKintosh, and A. J. Levine, Phys. Rev. E **68**, 025101 (2003); D. A. Head, A. J. Levine, and F. C. MacKintosh, *ibid.* **68**, 061907 (2003); Phys. Rev. Lett. **91**, 108102 (2003); C. Svaneborg, G. S. Grest, and R. Everaers, *ibid.* **93**, 257801 (2004).

[3] A. Tözeren and R. Skalak, J. Mater. Sci. **24**, 1700 (1989).

[4] D. J. Durian, Phys. Rev. Lett. **75**, 4780 (1995); **55**, 1739 (1997); S. A. Langer and A. J. Liu, J. Phys. Chem. B **101**, 8667 (1997); S. Tewari, D. Schiemann, D. J. Durian, C. M. Knobler, S. A. Langer, and A. J. Liu, Phys. Rev. E **60**, 4385 (1999).

[5] A. Yethiraj and A. van Blaaderen, Nature (London) **421**, 513 (2003); H. H. von Grünberg, P. Keim, K. Zahn, and G. Maret, Phys. Rev. Lett. **93**, 255703 (2004); A. Wille, F. Valmont, K. Zahn, and G. Maret, Euro. Phys. Lett. **57**, 219 (2002).

[6] H. M. Jaeger, S. R. Nagel, and R. P. Behringer, Rev. Mod. Phys. **68**, 1259 (1996).

[7] M. L. Falk and J. S. Langer, Annu. Rev. Condens. Matter Phys. **2**, 353 (2010).

[8] M. L. Falk and J. S. Langer, Phys. Rev. E **57**, 7192 (1998).

[9] L. D. Landau and E. M. Lifshitz, *Theory of Elasticity*, 3rd ed. (Pergamon Press, New York, 1986).

[10] P. Chaikin and T. Lubensky, *Principles of Condensed Matter Physics* (Cambridge University Press, Cambridge, 1995).

[11] J. E. Marsden and T. J. Hughes, *Mathematical Foundations of Elasticity* (Printice-Hall, Englewood Cliffs, NJ, 1968).

[12] B. A. DiDonna and T. C. Lubensky, Phys. Rev. E **72**, 066619 (2005).

[13] S. Sengupta, P. Nielaba, M. Rao, and K. Binder, Phys. Rev. E **61**, 1072 (2000); **61**, 6294 (2000).

[14] Z.-B. Wu, D. J. Diestler, R. Feng, and X. C. Zeng, J. Chem. Phys. **119**, 8013 (2003).

[15] A. Tanguy, J. P. Wittmer, F. Leonforte, and J. L. Barrat, Phys. Rev. B **66**, 174205 (2002).

[16] K. Zahn, A. Wille, G. Maret, S. Sengupta, and P. Nielaba, Phys. Rev. Lett. **90**, 155506 (2003).

[17] K. Franzrahe, P. Keim, G. Maret, P. Nielaba, and S. Sengupta, Phys. Rev. E **78**, 026106 (2008).

[18] K. Franzrahe, P. Nielaba, and S. Sengupta, Phys. Rev. E **82**, 016112 (2010).

[19] K.-Q. Zhang and X. Y. Liu, Langmuir **25**, 5432 (2009).

[20] P. Keim, G. Maret, U. Herz, and H. H. von Grünberg, Phys. Rev. Lett. **92**, 215504 (2004).

[21] V. J. Emery and J. D. Axe, Phys. Rev. Lett. **40**, 1507 (1978).

[22] He Li and George Lykotrafitis, Biophys. J. **102**, 75 (2012).

[23] Our definition of Ω implicitly assumes that fluctuations do not change the number and identity of the particles within the neighborhood since we study a network with a fixed topology of connections.

[24] Katalin Bagi, Int. J. Solids Struct. **43**, 3166 (2006).

[25] N. W. Ashcroft and N. D. Mermin, *Solid State Physics* (Holt, Rinehart, and Winston, New York, 1976).

[26] E. J. Garboczi and M. F. Thorpe, Phys. Rev. B **32**, 4513 (1985).

[27] Michael Tinkham, *Group Theory and Quantum Mechanics* (McGraw-Hill, New York, 1964).

[28] F. L. G. Picard, A. Ajdari, and L. Bocquet, Eur. Phys. J. E **15**, 371 (2004).

[29] A. S. Argon, Acta. Metall. **27**, 47 (1979).

[30] P. Schall, D. A. Weitz, and F. Spaepen, Science **318**, 1895 (2007).

[31] C. E. Maloney and A. Lemaïtre, Phys. Rev. Lett. **93**, 195501 (2004).

[32] M. Tsamados, A. Tanguy, F. Leonforte, and J. L. Barrat, Eur. Phys. J. E **26**, 283 (2008).

[33] This may have some similarities to the phenomenon of pressure induced amorphization, see, for e.g., R. Hemley, A. Jephcoat, H. Mao, L. C. Ming, and M. H. Manghnani, Nature (London) **334**, 52 (1988).

[34] Tamoghna Das, Surajit Sengupta, and Madan Rao, Phys. Rev. E **82**, 041115 (2010).